IEEE Access
Multidisciplinary ⋮ Rapid Review ⋮ Open Access Journal

Received 24 June 2023, accepted 20 August 2023, date of publication 1 September 2023, date of current version 11 September 2023.

Digital Object Identifier 10.1109/ACCESS.2023.3311319

RESEARCH ARTICLE

Deep Learning-Assisted Channel Estimation in Frequency Selective UWA Communication Systems

VAN DUC NGUYEN[1], DINH KHOA PHAN[1], AND TRINH VAN CHIEN[2], (Member, IEEE)
[1]School of Electrical and Electronics Engineering, Hanoi University of Science and Technology, Hanoi 100000, Vietnam
[2]School of Information and Communication Technology (SoICT), Hanoi University of Science and Technology, Hanoi 100000, Vietnam

Corresponding author: Trinh Van Chien (chientv@soict.hust.edu.vn)

This research is funded by Hanoi University of Science and Technology (HUST) under project number T2022-TT-001.

ABSTRACT Envisioned future wireless gives rise to the possibility of exploiting underwater applications with high spectral efficiency and reliable communication. This paper presents a method to combine channel estimation in the time domain with neural networks and supervised learning to improve orthogonal frequency-division multiplexing (OFDM) systems in underwater communications. The pilot structure is designed in such a way that the propagation channels are tracked from symbol to symbol. Moreover, the low-density parity-check code (LDPC) channel coding method is applied to overcome the severe fading and attenuation effects in underwater acoustic environments. We consider this proposed system's performance in a measurement-based channel model to evaluate it. In particular, the system's performance is evaluated for different levels of channel mobility. Numerical results show that, with the assistance of deep learning, the channel estimation performance can be improved, depending on how fast the channel changes. Compared with state-of-the-art benchmarks, our proposal offers better system performance in terms of bit error ratio and normalized mean square error.

INDEX TERMS UWA communications, supervised learning, frequency selective channels, OFDM, channel estimation.

I. INTRODUCTION

With the advent of the sixth generation (6G) communication networks, it will be possible to deploy underwater applications using fast and reliable acoustic connections [1], [2]. Thanks to the rapid development of new technologies, underwater acoustic (UWA) communication has attracted considerable recent attention from both academia and industry [3], [4]. UWA communication is more challenging than conventional radio communication in part because the propagation speed of acoustic waves in water, roughly 1500 [m/s] is much slower than that of radio waves [5]. For UWA propagation environments, this low speed of sound in water causes a significant delay spread, making the loss high and thus requiring a considerable guard length to compensate for the maximum delay and protect data over long propagation distances [6], [7]. The spectral efficiency and reliability of UWA communication systems are affected by the randomness of the underwater environments with various types of noises created by underwater animals. Consequently, the communication systems should be designed in such a way to cope with such fluctuations [8]. Therefore, analyzing a UWA communication system is usually tricky, especially in time-varying environments when the transceiver moves fast and suffers from Doppler effects [9], [10].

Like most communication channels, UWA propagation channels are unknown a priori and should be estimated in advance for signal detection and other purposed; so the role of channel estimation is of paramount importance [11]. For UWA communications, channel estimation in a frequency-selective environment becomes challenging due to nonstationary and impulsive noise [12], [13], [14]. In recent years, the orthogonal frequency-division multiplexing (OFDM) technique has been deployed to map

The associate editor coordinating the review of this manuscript and approving it for publication was Qingchun Chen.

frequency-selective channels into the corresponding static and frequency-flat ones with multiple subcarriers [15], [16]. Moreover, OFDM systems successfully eliminate inter-symbol interference (ISI) via orthogonal subcarriers to encode the transmitter signal and allow the subcarriers' signal spectrum to overlap. However, if the length of a signal sample is expanded, a time variation of the channels may arise in the signal sample, making OFDM systems sensitive to time-varying effects [17]. In a specific way, channel state information must be gathered to utilize multipath effects generated by many scatterers in the environment for equalization, and therefore demonstrating the signal recovery efficiently [18], [19]. Alternatively, in OFDM-based UWA communications systems, the propagation channels are often too complex to analyze and must be collected at the receiver to compensate for the propagation loss. To address this problem, pilot symbols known to both transmitter and receiver can be used, together with interpolation techniques to estimate the channels between the gap of two consecutive received pilot symbols. Even though linear minimum mean square error estimation offers channel estimates with high quality, preliminary information on channel statistics is costly to obtain due to high mobility [20]. In contrast, the least squares (LS) estimation method requires low computational complexity without any prior channel information. As a trade-off, it provides an initial estimated version of multi-path channels [17].

A variety of studies to improve performance, such as channel estimation, equalization, and channel coding have been applied for UWA systems. Some relevant channel coding techniques have been utilized in UWA communication systems to achieve specific objectives. In [21], convolutional codes and Reed Solomon codes were implemented for UWA systems by virtue of their simplicity. A turbo code was applied for a single-carrier UWA communication system with promising results in improving communication reliability in [22]. A comparison among four kinds of channel coding comprising the convolutional, turbo, polar, and low-density parity-check(LDPC) codes exhibits that excepting convolutional codes, the remaining channel coding techniques perform equivalently when the length of the data blocklength grows [23]. At a finite blocklength, LDPC codes have received much attention due to their outstanding performance in time and frequency selective fading channels. More specifically, an application of Quasi-Cyclic LDPC (QC-LDPC) codes in UWA communications was studied in [24], which indicates that the QC-LDPC can effectively improve the system efficiency. In addition, QC-LDPC codes have received significant attention in terms of hardware implementations of the encoding and decoding procedures. The 3GPP process has accepted the QC-LDPC as the standard channel coding scheme for 5G enhanced mobile broadband (eMBB) data channels [25].

Artificial intelligence has attracted considerable attention from academia and industry [26], [27] with its main purpose being introducing intelligence into systems via machine learning. In recent years, various machine learning algorithms have been introduced in wireless communication systems to solve critical problems [28], [29]. More specifically, deep learning methods have been introduced to enhance wireless communication systems' channel estimation and detection performance [30], [31]. In acoustic propagation environments, transmitted waves are absorbed by various factors through multi-path channels, obstacles, and animals. In practice, the channel impulse responses must be estimated precisely at the receiver to decode the transmitted signals. Note that minimum mean square error estimation is nontrivial to apply for acoustic environments with complex characteristics and lacking channel statistics given high mobility conditions. The other channel estimation methods are sub-optimal, which may produce high channel estimation errors as the received signal-to-noise ratio (SNR) is low. In order to improve the estimated quality of channel state information deep neural networks based on measurement data have been integrated into a canonical framework. As demonstrated in [32], the propagation channels themselves create certain patterns that match well with convolutional neural network (CNN) architectures. Consequently, CNNs have been deployed as one of the most common neural networks for channel estimation in UWA communications [33]. The correlation among channel coefficients brings superior advantages such as weight sharing, feature extraction and dimension reduction. CNNs can extract useful information from datasets in an input-to-output relation to predict desired results. Up to now, a few related works have been exploited data-driven approaches in general and CNN architectures for channel estimation purposes in UWA-OFDM communication systems [34], [35], [36]. However, to the best of our knowledge, no related work in the literature has investigated the support of CNNs for channel estimation in UWA-OFDM systems with the presence of channel coding.

This paper considers UWA-OFDM systems based on channel measurements comprising various characteristics and distortions. Even though it is difficult to simulate the channel as a probability distribution, the channel model can be mathematically approximated as in [37] that is effectively employed. Furthermore, LDPC coding is deployed to moderate the channel fading and attenuation effects in UWA communications. In principle, our main contributions are established in the system design and system performance evaluation, which are summarized as follows:

- The measurements take into account the effects of Doppler, propagation loss, and phase shifts. Using these perspectives, we develop a channel model based on measurements, aiming to minimize computational complexity while accurately representing the key characteristics of real propagation channels. Additionally, we propose a hybrid channel estimation approach that combines the efficiency of machine learning with traditional time domain channel estimation. This method involves training a CNN architecture to map channel estimates to their corresponding true channels.

- To compensate for propagation loss and frequency selective fading in UWA communications, we employ LDPC channel coding. By adopting the LDPC channel coding structure recommended by 3GPP, we not only enhance the receiver's ability to decode the intended signals but also ensure that the computational complexity remains within acceptable limits.
- Numerical results demonstrate the efficacy of the system design that combines channel coding and deep neural networks, evaluating its performance based on mean square error (MSE) and bit error ratio (BER). Additionally, we analyze the system's performance across various Doppler frequencies to showcase the robustness of the hybrid channel estimation method.

The rest of this paper is organized as follows: Section II presents in detail the considered UWA-OFDM system model over frequency-selective channels. In Section III, we describe the support of deep neural networks in improving the model-based channel estimation method, namely least squares. Section IV gives extensive numerical results to assess the system performance. Finally, Section V draws the main conclusions.

Notations: The regular transpose is denoted by the superscript $(\cdot)^T$. The notation $\text{mod}(\cdot,\cdot)$ is the modulo operation. $\mathsf{Pr}(\cdot)$ is the probability of an event. $\mathcal{CN}(\cdot,\cdot)$ denotes the circularly symmetric Gaussian distribution. $\mathcal{O}(\cdot)$ is the big-$\mathcal{O}$ notation that denotes the order of computational complexity. Moreover, $\|\cdot\|_F$ denotes the Frobenius norm of a matrix.

II. UWA-OFDM SYSTEM

This section presents a UWA system model, where a transmitter communicates with a receiver over a broadband time-frequency selective propagation environment. The transmitter and the receiver are equipped with a single antenna, and the signal processing architecture is illustrated in Fig. 1.

A. TRANSMITTER

In the data transmission phase, the data bit stream is divided into portions at the transmitter, each comprising K bits. Mathematically, let us denote each data portion as $\mathbf{c} = [c_1, \ldots, c_K]$, where $c_k \in \{0, 1\}$ is the k-th bit information of $\mathbf{c}$. The data bit portion $\mathbf{c}_k$ is fitted into the LDPC encoder to generate a vector $\mathbf{s}$ of N bits. Mathematically, we have the following relations

$$N = K/C_R, \tag{1}$$
$$K \leq \alpha Z_c. \tag{2}$$

where C_R is the code rate; the constant α represents the coding scheme suggested by the 3GPP [38]; and Z_c is denoted as the lifting size. Specifically, the two suggested schemes for the LDPC encoder are the first base graph (BG1) and the second base graph (BG2) with the detailed parameter settings: BG1 has C_R with $1/3 \leq C_R \leq 8/9$ and $\alpha = 22$; and BG2 with $1/5 \leq C_R \leq 2/3$ and α is

$$\alpha = \begin{cases} 10, & \text{if } K > 640, \\ 9, & \text{if } 560 < K \leq 640, \\ 8, & \text{if } 192 < K \leq 560, \\ 6, & \text{elsewhere.} \end{cases} \tag{3}$$

For the given length of data portions K and the LDPC coding scheme, i.e., either BG1 or BG2, we formulate the parity check matrix $\mathbf{H}$ based on the following steps

1) For given K and α, Z_c is approximately selected, which is closest to K/α, by utilizing [38, Table 5.3.2-1] and then the set index i_{LS} is further defined.
2) From the value of i_{LS}, the lifting matrix $\mathbf{H}_{\text{BG}}$ can be defined as

$$[\mathbf{H}_{\text{BG}}]_{ij} = \begin{cases} -1, & \text{if } V_{ij} = -1, \\ P_{ij}, & \text{elsewhere.} \end{cases} \tag{4}$$

where $[\mathbf{H}_{\text{BG}}]_{ij}$ denotes the (i, j)-th element of matrix $\mathbf{H}_{\text{BG}}$; V_{ij} is the lifting coefficient, which is defined by utilizing [38, Table 5.3.2-2] for BG_1 and by utilizing [38, Table 5.3.2-3] for BG_2; and $P_{ij} = \text{mod}(V_{ij}, Z_c)$, $\forall i, j$ satisfied $V_{ij} \neq -1$. We note that the matrix $\mathbf{H}_{\text{BG}}$ is of size $m_b \times n_b$, which depends on the LDPC coding scheme either BG1 or BG2.
3) The parity check matrix $\mathbf{H}$ of size $m_b Z_c \times n_b Z_c$ is extended from $\mathbf{H}_{\text{BG}}$ by: *i*) replacing each element with value -1 by a zero matrix of size $Z_c \times Z_c$; and *ii*) replacing each element with value P_{ij} by a cicular permutation matrix $\mathbf{C}_{ij}$ of size $Z_c \times Z_c$, where $\mathbf{C}_{ij}$ is attained by circularly shifting the identity matrix $\mathbf{I}_{ij}$ of size $Z_c \times Z_c$ to the right P_{ij} times. We note that the size of the parity check matrix $\mathbf{H}$ satisfies $n_b Z_c = K + m_b Z_c$.
4) For the sake of convenience in encoding, the parity check matrix is decomposed into as

$$\mathbf{H} = \begin{bmatrix} \mathbf{A} & \mathbf{B} & \mathbf{0} \\ \mathbf{D} & \mathbf{E} & \mathbf{I} \end{bmatrix}. \tag{5}$$

where the matrix $\mathbf{A}$ and $\mathbf{I}$ is of size $oZ_c \times \alpha Z_c$ with o being a portion of the number of parity bits; the matrix $\mathbf{B}$ is of size $oZ_c \times oZ_c$; the matrix $\mathbf{0}$ is of size $oZ_c \times (m_b - o)Z_c$; the matrix $\mathbf{D}$ is of size $(m_b - o)Z_c \times \alpha Z_c$; the matrix $\mathbf{E}$ is of size $(m_b - o)Z_c \times oZ_c$; and $\mathbf{I}$ is the identity matrix of size $(m_b - o)Z_c \times (m_b - o)Z_c$.

Let us denote the vector $\mathbf{s} = [\mathbf{c}, \mathbf{p}_a, \mathbf{p}_c]^T$ of size $K + m_b Z_c$ with $\mathbf{c} = [c_1, \ldots c_K]^T$, $\mathbf{p}_a = [p_{a1}, \ldots, p_{ao}]^T$, and $\mathbf{p}_c = [p_{c1}, \ldots, p_{c(m_b-o)}]^T$. Here, the vectors $\mathbf{p}_a$ and $\mathbf{p}_c$ involve the parity bits, which are designed by the following equation $\mathbf{Hs} = \mathbf{0}$. From (5), we obtain a system of equations as follows

$$\mathbf{Ac} + \mathbf{Bp}_a + \mathbf{0p}_c = \mathbf{0}, \tag{6}$$
$$\mathbf{Dc} + \mathbf{Ep}_a + \mathbf{Ip}_c = \mathbf{0}. \tag{7}$$

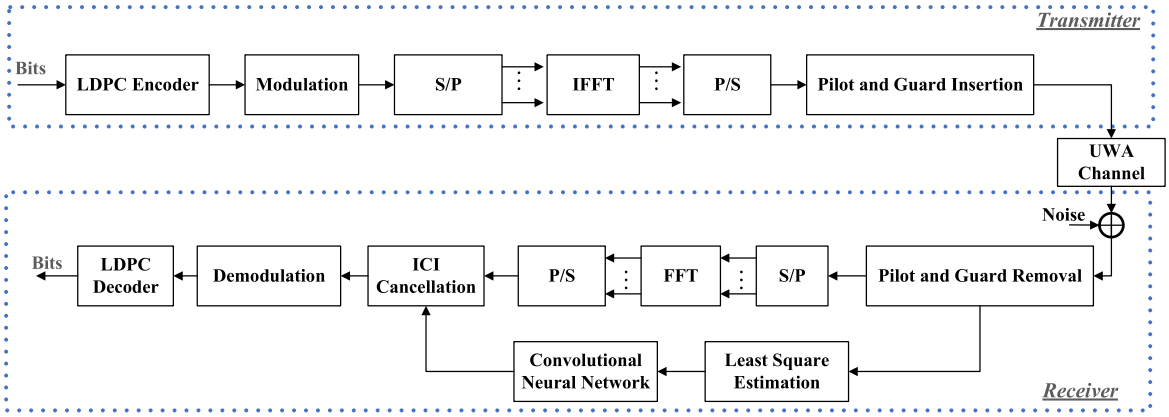

FIGURE 1. The considered system model over a UWA communication environment.

Conditioned on the full rank of matrix $\mathbf{B}$, the solution to $\mathbf{p}_a$ and $\mathbf{p}_c$ is respectively expressed as

$$\mathbf{p_a} = \mathbf{B}^{-1}\mathbf{A}\mathbf{c}, \tag{8}$$

$$\mathbf{p_c} = \mathbf{D}\mathbf{c} + \mathbf{E}\mathbf{B}^{-1}\mathbf{A}\mathbf{c}. \tag{9}$$

After that, the vector $\mathbf{s}$ is processed by the low density parity check coding algorithm [38, Section 5.3.2] so that the encoded codeword is $\mathbf{u} = [\mathbf{c}_{2Z_c-1}, \ldots, \mathbf{c}_K, \mathbf{p}_a, \mathbf{p}_c]^T$ of size $(m_b - 2)Z_c + K$. Hence, from (1), we obtain $N = (m_b - 2)Z_c + K = K/C_R$. The encoded codeword $\mathbf{u}$ is fed into the modulation module, say M-QAM (quadrature amplitude modulation). This module will convert the binary bits into modulated signals by a finite constellation set comprising the M points. In order to handle the frequency selective issue, the system divides the given system bandwidth B into N_c sub-carriers where the channels are frequency flat. The codeword $\mathbf{u}$ is converted from frequency domain to time domain by exploiting inverse fast Fourier transform (IFFT) with the support of the serial-to-parallel (S/P) and parallel-to-serial (P/S) modules. Mathematically, let us define $\tilde{N}$ the number of OFDM symbols, then it holds that

$$N = \tilde{N} N_c \log_2 M. \tag{10}$$

The n-th OFDM symbol in the frequency domain, denoted by $\mathbf{x}^n$ is constructed as

$$\mathbf{x}^n = [x_0^n, x_1^n, \ldots, x_{N_c-1}^n]^T. \tag{11}$$

then the IFFT module will transform this signal to the time domain, following by the pilot insertion module, which is later utilized for the channel estimation at the receiver. The pilot signal, denoted by $\tilde{\mathbf{p}}^n$, includes $2N_G + 1$ samples, which is constructed as

$$\tilde{\mathbf{p}}^n = \left[\underbrace{0, \cdots, 0}_{N_G \text{ zeros}}, \tilde{p}^n, \underbrace{0, \cdots, 0}_{N_G \text{ zeros}}\right]^T. \tag{12}$$

where $\tilde{p}^n$ is the complex pilot samples allocated to the n-th OFDM symbol. In (12), the first N_G zero samples contribute as the guard interval, while the last N_G zero samples will be utilized to cope with the multipath effects. Note that N_G should be larger than the number of multipaths, i.e., alternatively called the length of channel impulse response. Let us denote $\tilde{\mathbf{x}}^n = [\tilde{x}_0^n, \tilde{x}_1^n, \ldots, \tilde{x}_{N_c-1}^n]^T$ is the n-th OFDM symbol in time domain, then the represented signal after the pilot & guard insertion module is $[\tilde{\mathbf{p}}^n, \tilde{\mathbf{x}}^n]^T$ with the size $N_{\text{sym}} = N_c + 2N_G + 1$.

TABLE 1. UWA channel parameter measurements provided in [37] with the 30 path gains.

Path gain	Doppler Freq.	Path gain	Doppler Freq.
1	7.7126	0.1267	-0.3665
0.4296	5.9475	0.1085	-0.9089
0.5763	5.5495	0.1072	-1.5021
0.5130	5.9136	0.0955	-2.1927
0.3770	4.3182	0.1377	-2.7172
0.3167	3.9724	0.1514	-3.1276
0.3122	3.2483	0.1276	-3.7829
0.3426	3.0197	0.1571	-3.7057
0.2407	3.4004	0.1684	-4.6817
0.2035	3.1037	0.1348	-5.3018
0.1978	2.7241	0.0527	-5.4819
0.1491	2.1228	0.0735	-5.6878
0.1885	1.5381	0.0820	-5.9273
0.1685	0.9626	0.1026	-6.1064
0.1645	0.2817	0.0525	-5.9629

B. UWA CHANNEL MODEL

In this paper, we exploit the time-variant channel impulse response model [39] to acquire the channel as follows

$$g(\tau, t) = \frac{1}{\sqrt{L}} \sum_{l=0}^{L-1} \frac{1}{\sqrt{N_l}} \sum_{n=1}^{N_l} c_{n,l} e^{j(2\pi f_{n,l} t + \theta_{n,l})} \delta(\tau - \tau_l). \tag{13}$$

where τ and t denote the delay spread and time instance, respectively; L is the number of propagation paths, each having a separate delay τ_l; N_l is the number of paths with the same delay spread τ_l. In the N_l paths, the n-th path is characterized by the Doppler frequency $f_{n,l}$, the path gain $c_{n,l}$, and the phase shift $\theta_{n,l}$. We stress that the channel impulse response in (13) can be applied for various wide-band propagation environments with different mobility and phase shifts. For a specific UWA propagation environment, the set

of parameters $\mathcal{A}_l = \{N_l, c_{n,l}, f_{n,l}, \theta_{n,l}\}$ can be determined by matching the model (13) with the measurement data. For the l-th path, let us define the time-complex channel $u_l(t)$ as

$$u_l(t) = \sum_{n=1}^{N_l} c_{n,l} e^{j(2\pi f_{n,l} t + \theta_{n,l})}. \tag{14}$$

then the optimized set $\mathcal{A}_l$ is attained as the solution of the following optimization problem

$$\begin{aligned} \underset{\{N_l, c_{n,l}, f_{n,l}, \theta_{n,l}\}}{\text{minimize}} \quad & \left(\frac{1}{t_{\max}} \int_0^{t_{\max}} |u_l(t) - \hat{u}_l(t)|^p dt \right)^{1/p} \\ \text{subject to} \quad & 0 \le \theta_{n,l} \le 2\pi, \forall n, \\ & f_{n,l} \le 0, \forall n, \\ & 0 \le c_{n,l} \le 1, \forall n, \\ & N_l \in \mathbb{N}. \end{aligned} \tag{15}$$

where p represents the ℓ_p-norm, $t_{\max}$ is the maximum time instance, and $\hat{u}_l(t)$ represents the measurement of the time-complex channel $u_l(t)$, which is shown in Table 1. The practical aspects of problem (15) are given in Remark 1.

Remark 1: Unlike most previous works in the literature, our work investigates the system performance based on channel modeling with practical features. Specifically, the time-variant channel model is matched to real UWA propagation environments by considering problem (15) over a sufficiently large dataset comprising many different propagation paths. One can obtain the solution to problem (15) by, for example, the ℓ-norm optimization approach.

C. RECEIVER

After the signals are transmitted over the UWA environment, the received signal $y^n(i), \forall i = 1, \ldots, N_{\text{sym}} - 1$ related to the n-th OFDM symbol and the i-th sampling interval is formulated as

$$y^n(i) = \sum_{l=0}^{L-1} g^n(l, i) x^n(i - l) + w^n(i). \tag{16}$$

where $g^{(n)}(l, i)$ is the corresponding channel impulse response; and $w^n(i)$ is additive white Gaussian noise distributed as $w^n(i) \sim \mathcal{CN}(0, \sigma^2)$ with σ^2 being the noise power. By removing the guard interval and pilot signals, the received signal in the frequency domain is given as follows

$$\begin{aligned} Y^n(k) &= \frac{1}{N_c} \sum_{i=0}^{N_c-1} y^n(i) e^{-j2\pi ki/N_c} \\ &\overset{(a)}{=} \sum_{m=0}^{N_c-1} \sum_{l=0}^{L-1} X^n(m) G_l^n(m - k) e^{-j2\pi lm/N_c} \\ &\quad + W^n(k), k = 0, \cdots, N_c - 1. \end{aligned} \tag{17}$$

where (a) is obtained by exploiting $y^n(i)$ in (16). Moreover, $W^n(k)$ and $G_l^n(k)$ are the Fourier transform of the noise $w^n(i)$ and the channel impulse response $g^n(l, i)$, respectively. In more detail, $G_l^n(k)$ is mathematically formulated as

$$G_l^n(k) = \frac{1}{N_c} \sum_{m=0}^{N_c-1} g^n(l, m) e^{-j2\pi mk/N_c}. \tag{18}$$

Consequently, the received signal in the frequency domain, denoted by $\mathbf{Y}^n \in \mathbb{C}_c^N$ is defined as

$$\mathbf{Y}^n = \mathbf{G}^n \mathbf{X}^n + \mathbf{W}^n. \tag{19}$$

where the following definitions hold

$$\mathbf{Y}^n = [Y^n(0), Y^n(1), \ldots, Y^n(N_c - 1)]^T, \tag{20}$$

$$\mathbf{X}^n = [X^n(0), X^n(1), \ldots, X^n(N_c - 1)]^T, \tag{21}$$

$$\mathbf{W}^n = [W^n(0), W^n(1), \ldots, W^n(N_c - 1)]^T. \tag{22}$$

which is the vector of received signal, transmitted signal, and noise, respectively. Meanwhile, the channel matrix of the n-th OFDM symbol, denoted by $\mathbf{G}^n \in \mathbb{C}^{N_c \times N_c}$, is

$$\mathbf{G}^n = \begin{bmatrix} b_{0,0} & b_{0,1} & \cdots & b_{0,N_c-1} \\ b_{1,0} & b_{1,1} & \cdots & b_{1,N_c-1} \\ \vdots & \vdots & \cdots & \vdots \\ b_{N_c-1,0} & b_{N_c-1,1} & \cdots & b_{N_c-1,N_c-1} \end{bmatrix}. \tag{23}$$

where the (m, k)-th element of matrix $\mathbf{G}^n$, say $b_{m,k}$, is defined as follows

$$b_{m,k} = \sum_{l=0}^{L-1} G_l^n(k - m) e^{-j2\pi ml/N_c}, m, k = 0, 1, \cdots, N_c - 1. \tag{24}$$

We note that if the channel impulse responses are static, i.e., time-invariant in each OFDM symbol, then the channel matrix $\mathbf{G}^n$ in (23) is approximately a diagonal matrix. For the time-invariant channels, the ICI components disappear as the off-diagonal elements $b_{m,k}, \forall m \neq k$, are zeros. The orthogonality of the sub-carriers is preserved and the desired signal is obtained at the receiver as follows

$$\mathbf{X}^n = (\mathbf{G}^n)^{-1} \mathbf{Y}^n. \tag{25}$$

which is low computational complexity since it is straightforward to obtain the inversion of a diagonal matrix. Nonetheless, in UWA communications, the channel impulse responses are time-variant due to, for example, the fast movement of the transceiver. For such, the channel matrix in (23) is nondiagonal. Besides, the orthogonality of the subcarriers is broken down because of the rapid change of the propagation channels in the time domain and the Doppler shifts. The nondiagonality of the channel matrix $\mathbf{G}^n$ introduces inter-carrier interference. It is nontrivial to compute the matrix inverse in this phenomenon, especially it becomes problematic with a rapid change of the channel impulse responses, which require a large number of subcarriers. There are fortunately a small number of non-zero elements in $\mathbf{G}^n$, while most of its elements are zeros due to the finite value of the maximum Doppler frequency. The sparsity, which $\mathbf{G}^n$ creates, makes a banded matrix and acquires an

opportunity to compute the matrix inverse with a low cost.[1] We set $b_{m,k} = 0$ at for the elements distant from the main diagonal of the channel matrix $\mathbf{G}^n$ as defined in (26), as shown at the bottom of the next page. The expression in (26) indicates that $b_{m,k} = 0$ if $|k - m| \geq q/2$, where q is the size of the banded matrix $\mathbf{G}^n$. We emphasize that the banded size q represents the number of dominant inter-carrier interference terms. The inverse matrix of the banded matrix can be obtained by applying, for example [40] with the computational complexity in the order of $\mathcal{O}(2qN_c^2)$.[2] The signal $\mathbf{X}^n$ is then demodulated to obtain the output data $\mathbf{D}^n$ comprising both the information of data bits and parity bits.

We now borrow the generalized minimum-sum decoding algorithm using a linear approximation (LAMS) [41] to construct the LDPC decoder. Note the parity check matrix $\mathbf{H}$ is sparse in the sense that it only includes the binary elements and the number of ones, denoted by $\tilde{J}$, is much less than $m_b n_b Z_c^2$. The matrix $\mathbf{H}$ is presented by a bipartite graph comprising $n_b Z_c$ variable nodes, $v_j, \forall j = 0, \ldots, n_b Z_c - 1$; $m_b Z_c$ check nodes, $c_i, \forall i = 0, \ldots, m_b Z_c - 1$; and $\tilde{J}$ edges $e_{\tilde{j}}, \forall \tilde{j} = 0, \ldots, \tilde{J} - 1$. In principle, the i-th check node is connected to the j-th variable node by the j-th edge if the (i, j)-th element of the matrix $\mathbf{H}$ equals to one. The following definitions hold

i) The neighbors of the variable node v_j include the check nodes $c_i, \forall i \in \mathcal{C}(j)$, where the set $\mathcal{C}(j)$ comprises the indices of all the check nodes that connect to the variable node v_j.

ii) The neighbors of the check node c_i include the variable nodes $v_j, \forall j \in \mathcal{V}(i)$, where the set $\mathcal{V}(i)$ comprises the indices of all the variable nodes that connect to the check node c_i.

Based on the minimum-sum method, which is a simplified version of the belief propagation, the initialization of the channel log-likelihood ratio (LLR) of the j-th bit, denoted by $L_j^{(0)}$, is defined as follows

$$L_j^{(0)} = \log\left(\frac{\mathsf{Pr}\left(u_j^{(0)} = 0|d\right)}{\mathsf{Pr}\left(u_j^{(j)} = 1|d\right)}\right) = d. \tag{27}$$

where d is a data symbol belonging to the output data $\mathbf{D}^n, \forall n$; the data symbol d involves several bits that are related the encoded bits, defined at the initial stage $\{u_j^{(0)}\}$; $\mathsf{Pr}(u_j^{(0)} = 0|d)$ and $\mathsf{Pr}(u_j^{(0)} = 0|d)$ are the conditional probabilities that decide $u_j^{(0)} = 0$ or $u_j^{(0)} = 1$ for given d. We use the LLR expression in (27) to design a belief propagation decoding in an iterative manner. In particular, the LLR propagates from the variable node v_j to its neighbor check node $c_i, \forall i \in \mathcal{C}(j)$, is initially given as $L_{j\to i}^{(0)} = L_j^{(0)}$. At iteration v, the check node c_i receives the LLR information $L_{j\to i}^{(v)}$ from the neighbor nodes $v_j, \forall j \in \mathcal{V}(i)$. In the minimum-sum (MS) algorithm, the backward LLR from the check node c_i to its neighbor variable node v_j is formulated as follows

$$L_{i\to j}^{(v)} = \left(\prod_{j'\in\mathcal{V}(i)\setminus\{j\}} \text{sign}\left(L_{j'\to i}^{(v)}\right)\right) \min_{j'\in\mathcal{V}(i)\setminus\{j\}} \left(\left|L_{j'\to i}^{(v)}\right|\right). \tag{28}$$

where sign$(\cdot)$ is the function that obtains the sign of a number. In order to yield a better performance than the MS algorithm, one can introduce the nomalized MS (NMS) algorithm as

$$L_{i\to j}^{(v)} = \alpha^{(v)} \left(\prod_{j'\in\mathcal{V}(i)\setminus\{j\}} \text{sign}\left(L_{j'\to i}^{(v)}\right)\right) \times \min_{j'\in\mathcal{V}(i)\setminus\{j\}} \left(\left|L_{j'\to i}^{(v)}\right|\right). \tag{29}$$

where $\alpha^{(v)}$ is the normalized factor. Alternatively, we can introduce the offset MS (OMS) algorithm that can also boost the performance of the MS algorithm by an offset factor $\beta^{(v)}$ as follows

$$L_{i\to j}^{(v)} = \left(\prod_{j'\in\mathcal{V}(i)\setminus\{j\}} \text{sign}\left(L_{j'\to i}^{(v)}\right)\right) \times \max\left(\min_{j'\in\mathcal{V}(i)\setminus\{j\}} \left(\left|L_{j'\to i}^{(v)}\right|\right) + \beta^{(v)}, 0\right). \tag{30}$$

Combining (28)–(30), a linear approximation of the amplitude $|L_{j'\to i}^{(v)}|$ can be obtained. Accordingly, the backward LLR from the check node c_i to its neighbor variable node v_j is formulated as follows

$$L_{i\to j}^{(v)} = \left(\prod_{j'\in\mathcal{V}(i)\setminus\{j\}} \text{sign}\left(L_{j'\to i}^{(v)}\right)\right) \times \max\left(\alpha^{(v)} \min_{j'\in\mathcal{V}(i)\setminus\{j\}} \left(\left|L_{j'\to i}^{(v)}\right|\right) + \beta^{(v)}, 0\right). \tag{31}$$

After that, the current channel LLR at iteration v is computed as follows

$$L_j^{(v)} = \text{sign}\left(L_j^{(0)}\right) \max\left(\tilde{\alpha}^{(v)}\left|L_j^{(0)}\right| + \tilde{\beta}^{(v)}, 0\right) + \sum_{i\in\mathcal{C}(j)} L_{i\to j}^{(v)}. \tag{32}$$

where $\tilde{\alpha}^{(v)}$ and $\tilde{\beta}^{(v)}$ are the adjusting factors that can be adaptive to the iterations. The LLR information from the check node c_i to the neighbor node v_j is updated for the next iteration as follows

$$L_{j\to i}^{(v+1)} = L_j^{(v)} - L_{i\to j}^{(v)}. \tag{33}$$

The encoded bits $u_j^{(v)}, \forall j$, are defined at iteration v as follows

$$u_j^{(v)} = \begin{cases} 1, & \text{if } L_j^{(v)} \leq 0, \\ 0, & \text{if } L_j^{(v)} > 0. \end{cases} \tag{34}$$

[1] A banded matrix is a sparse matrix, whose non-zero elements are on the diagonal band that are main diagonal elements and off-diagonal elements on the either sides.

[2] By exploiting the Cholesky decomposition, computing the inversion of matrix $\mathbf{G}^n \in \mathbb{C}^{N_c\times N_c}$ requires the computational complexity in the order of $\mathcal{O}(0.5N_c^3)$, and therefore the banded matrix reduces the cost significantly as N_c is large or q is small.

We stress that the LPDC decoding process will be terminated if $\mathbf{Hu}^{(v)} = \mathbf{0}$, where $\mathbf{u}^{(v)}$ is the vector gathering all the decoded bits $u_j^{(v)}$. In this case, there are no bit errors. Otherwise, the LPDC decoding process reaches the maximum number of iterations and the system suffers from the error decoding.

III. CNN-AIDED CHANNEL ESTIMATION

This section first exploits the least squares channel estimation to obtain initial channel estimates. After that, the channel estimation errors are reduced by utilizing supervised learning to train a convolutional neural network.

A. PILOT STRUCTURE IN TIME DOMAIN CHANNEL ESTIMATION

In order to decode the desired signals sent by the transmitter over the UWA environment, the system should estimate the propagation channels. In this paper, we apply the pilot structure in Fig. 2, each OFDM comprising the N_G zero symbols dedicated to the guard interval to mitigate inter-symbol interference, one pilot symbol, and N_G zero symbols to compensate the multi-path effects from channel impulse responses. We stress that these zero symbols protect the received pilot signal not overlapped with the data symbols. Mathematically, the guard interval, denoted by T_G, is selected so that $T_G \geq \tau_{\max}$, where $\tau_{\max}$ is the maximum propagation delay. As a consequence, the received pilot symbols are located in the pilot guard interval as shown in Fig. 2.

The pilot signal in a received OFDM symbol is observed at the sampling index n_p with $N_G \leq n_p \leq N_G + l$, where l is the multiple-path index satisfied $0 \leq l \leq L-1$. Corresponding to the n-th transmit OFDM symbol, the received pilot signal at the n_p sampling index is formulated as follows

$$y^n(n_p) = \sum_{l=0}^{L-1} g^n(l, n_p)\tilde{p}^n + w^n(n_p). \tag{35}$$

where $\tilde{p}^n$ is the complex pilot sample defined in (12); and $w_p^n(n_p)$ is AWGN at this sampling index. As illustrated in Fig. 2, each transmitted OFDM symbol has one non-zero pilot symbol and $2N_G$ zero samples in the pilot structure, which protect the non-zero pilot symbol from the multi-path effects. The information of scattering paths are evaluated from the received pilot signals. The interpolation is utilized to reconstruct the channel information from the received pilot

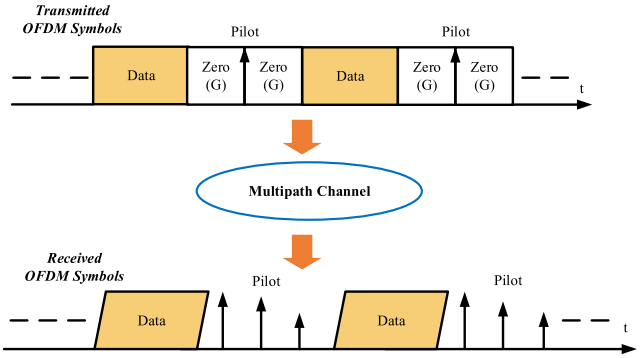

FIGURE 2. The visualization of the pilot structure in each OFDM utilized for UWA environment.

symbols. After estimating the propagation channels in time domain, the estimated channel matrix is of size $L \times N_{sym}$ defined as follows

$$\tilde{\mathbf{g}}^n = \begin{bmatrix} \tilde{g}^n(0,0) & \tilde{g}^n(0,1) & \dots & \tilde{g}^n(0,N_{\text{sym}}-1) \\ \tilde{g}^n(1,0) & \tilde{g}^n(1,1) & \dots & \tilde{g}^n(1,N_{\text{sym}}-1) \\ \vdots & \vdots & \dots & \vdots \\ \tilde{g}^n(L-1,0) & \tilde{g}^n(L-1,1) & \dots & \tilde{g}^n(L-1,N_{\text{sym}}-1) \end{bmatrix}. \tag{36}$$

where $\tilde{g}^n(l,n)$ is the channel estimate of the true channel $g^n(l,n), \forall l = 0, \cdots L-1, n = 0, \cdots, N_{\text{sym}}-1$. The matrix $\mathbf{G}^n$ in frequency domain, formulated in (26), is computed by exploiting the FFT transform of matrix $\tilde{\mathbf{g}}^n$ after removed pilot. From the matrix $\mathbf{G}^n$, we borrow the suggested method in [42] to mitigate inter-carrier interference.

In this paper, we interpolate the propagation channels for all the subcarriers by the curve fitting technique as illustrated in Fig. 3. From (35), in the n-th OFDM symbol, the channel impulse response regarding the l-th scattering path and the n_p-th sampling index can be obtained by using the least squares estimation as follows

$$\tilde{g}^n(l, n_p) = y^n(n_p)/\tilde{p}^n. \tag{37}$$

We notice that the channel estimate $\tilde{g}^n(l, n_p)$ in (36) obtained by the least squares estimation contaminated by noise. For the sake of simplicity and for a low computational complexity design, we utilize the linear interpolation in time domain so that the channel impulse response of the n_{inter}-th sampling

$$\mathbf{G}^n = \begin{bmatrix} b_{0,0} & b_{0,1} & \dots & b_{0,q/2} & 0 & 0 & 0 \\ b_{1,0} & b_{1,1} & \dots & \dots & \dots & 0 & \vdots \\ \vdots & \vdots & \dots & \dots & \dots & \dots & 0 \\ b_{q/2,0} & \dots & \dots & \dots & \dots & \dots & b_{N_c-1-q/2,N_c-1} \\ 0 & \dots & \dots & \dots & \dots & \dots & \vdots \\ \vdots & \vdots & \dots & \dots & \vdots & b_{N_c-2,N_c-2} & b_{N_c-2,N_c-1} \\ 0 & 0 & 0 & b_{N_c-1,N_c-1-q/2} & \dots & b_{N_c-1,N_c-2} & b_{N_c-1,N_c-1} \end{bmatrix}. \tag{26}$$

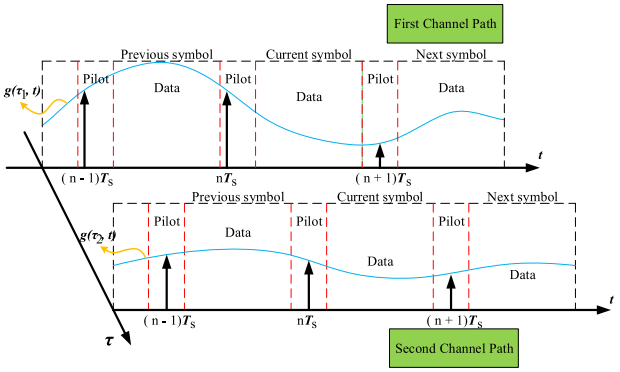

FIGURE 3. All the channel impulse responses are obtained by the curve fitting technique.

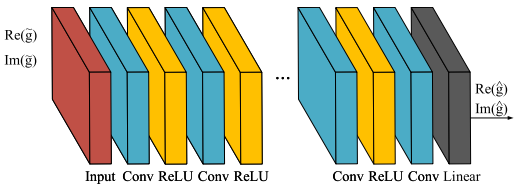

FIGURE 4. The proposed CNN structure for channel estimation in UWA environment.

index with $n_p \leq n_{\text{inter}} \leq n_{p+1}$ and n_{p+1} implying the index of the non-zero pilot symbol of the $(n+1)$-th OFDM symbol, is computed as follows

$$\tilde{g}^n(l, n_{\text{inter}}) = \tilde{g}^n(l, n_p) + \left(\tilde{g}^{n+1}(l, n_p) - \tilde{g}^n(l, n_p)\right) \times \frac{(n_{\text{inter}} - n_p)}{N_{\text{sym}}}. \tag{38}$$

where $\tilde{g}^{n+1}(l, n_p)$ is the channel estimate of the true version $g^{n+1}(l, n_p)$ in the $(n+1)$-th OFDM symbol.

B. CNN-AIDED CHANNEL ESTIMATION

It should be emphasized that the propagation paths in (13) are complex numbers, and we must point out that the channel gains are bounded from above to exploit a neural network to boost the channel estimation quality. By using the frequency selective channel model in (13), it holds that

$$\begin{aligned} |g(\tau, t)| &= \\ &\frac{1}{\sqrt{L}} \left| \sum_{l=0}^{L-1} \frac{1}{\sqrt{N_l}} \sum_{n=1}^{N_l} c_{n,l} e^{j(2\pi f_{n,l} t + \theta_{n,l})} \delta(\tau - \tau_l) \right| \\ &\overset{(a)}{\leq} \frac{1}{\sqrt{L}} \sum_{l=0}^{L-1} \frac{1}{\sqrt{N_l}} \sum_{n=1}^{N_l} \left| c_{n,l} e^{j(2\pi f_{n,l} t + \theta_{n,l})} \delta(\tau - \tau_l) \right| \\ &\overset{(b)}{=} \frac{1}{\sqrt{L}} \sum_{l=0}^{L-1} \frac{1}{\sqrt{N_l}} \sum_{n=1}^{N_l} \left| c_{n,l} \right|, \end{aligned} \tag{39}$$

where (a) is obtained due to the triangle inequality, and (b) is because the unit modulus, i.e., $|e^{jx}| = 1, \forall x$. From (39), it manifests that $|g(\tau, t)|$ is bounded, and therefore one can design a neural network for learning and supporting the channel estimation module as a consequence of the universal approximation theorem.

Each estimated channel matrix $\tilde{\mathbf{g}}^n$ constructs the correlation in the time domain and when the paths are close to each other. Observing that a fully-connected neural network does not capture such correlation. Consequently, many weights and biases must be trained, requiring high computational complexity. Furthermore, a neuron in each hidden layer of fully-connected neural networks should regularly connect all the neurons in the previous layer. This neural network easily suffers from the overfitting issue. Thanks to the matrix structure constructed in (36), in this paper, we construct and train a CNN after exploiting time domain channel estimation to minimize mean square error (MSE) between the channel estimates and the original channels. The CNN structure used for our purposes is illustrated in Fig. 4. The proposed neural network includes the four different kinds of layers: the input layer, the convolutional layers, the rectified linear unit (ReLU) activation layer, and the linear layer. The model includes $\tilde{L}$ convolutional layers. Each layer $l \in \tilde{L}$ includes z_l sliding window kernel of size $k_l \times k_l$ will be convolutioned with the Input Layer $I \in \mathbb{R}^{x_{l-1} \times y_{l-1} \times z_{l-1}}$, where $x_{l-1} \times y_{l-1}$ are the size of the convolutional layer $l-1$. After each convolutional layer, we use activation function ReLU. Each matrix $\tilde{\mathbf{g}}^n \in \mathbb{C}^{L \times N_{\text{sym}}}$ is considered to formulate the input. Neural networks are canonically constructed for real data, so the channel estimate $\tilde{\mathbf{g}}^n$ is split into the real and imaginary parts as follows

$$T = \left(\mathsf{Re}[\tilde{\mathbf{g}}^n], \mathsf{Im}[\tilde{\mathbf{g}}^n]\right). \tag{40}$$

where $\mathsf{Re}[\cdot]$ and $\mathsf{Im}[\cdot]$ yield the real and imaginary part of a complex number. Similarly, the corresponding output is defined as

$$O = \left(\mathsf{Re}[\hat{\mathbf{g}}^n], \mathsf{Im}[\hat{\mathbf{g}}^n]\right). \tag{41}$$

where $\hat{\mathbf{g}}^n$ is the output of the CNN. The training process performs the following mapping

$$\left(\mathsf{Re}[\tilde{\mathbf{g}}^n], \mathsf{Im}[\tilde{\mathbf{g}}^n]\right) \rightarrow \left(\mathsf{Re}[\hat{\mathbf{g}}^n], \mathsf{Im}[\hat{\mathbf{g}}^n]\right). \tag{42}$$

with $\tilde{\mathbf{g}}^n$ being the time domain channel estimation produced by the least squares method in (36) and $\hat{\mathbf{g}}^n$ is its refined version by the CNN.

Since the ultimate goal of our CNN is to minimize the MSE between the channel estimates and their true versions, the loss function is defined as

$$\mathcal{L}(W, B) = \frac{1}{\tilde{N}} \sum_{n=1}^{\tilde{N}} \left\| \hat{\mathbf{g}}^n - \mathbf{g}^n \right\|_F^2. \tag{43}$$

where W and B are the weights and bias, respectively. Due to [43], the complexity of the convolutional layers can be calculated as $\mathcal{O}(\sum_{l \in \tilde{L}} x_l y_l k_l^2 z_l z_{l-1})$. Therefore, the linear layer will compute $x_L y_L z_l x_{\text{linear}} y_{\text{linear}}$ multiplications with $x_L \times y_L$ and $x_{\text{linear}} \times y_{\text{linear}}$ are the size of the last convolution layer and the linear layer. Note that we apply the CNN for the sequential OFDM symbols, so the sizes of the convolutional

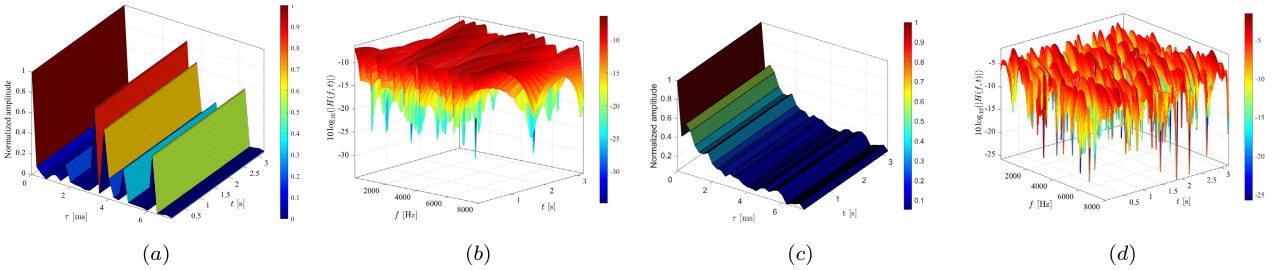

(a) (b) (c) (d)

FIGURE 5. The properties of the channel measurements: (*a*) The channel impulse response $h(\tau, t)$ with the maximum Doppler frequency $f_{\mathrm{D,max}} = 2$ [Hz]; (*b*) The channel in frequency domain $H(f, t)$ with the maximum Doppler frequency $f_{\mathrm{D,max}} = 2$ [Hz]; (*c*) The channel impulse response $h(\tau, t)$ with the maximum Doppler frequency $f_{\mathrm{D,max}} = 8$ Hz; and (*d*). The channel in frequency domain $H(f, t)$ with the maximum Doppler frequency $f_{\mathrm{D,max}} = 8$ [Hz].

layer and the linear layer are $2L \times N_{\mathrm{sym}}$. The computational complexity of the proposed CNN is obtained in the order of

$$\mathcal{C}_{\mathrm{CNN}} = \mathcal{O}\left(4z_L L^2 N_{\mathrm{sym}}^2 + 2LN_{\mathrm{sym}} \sum_{l=1}^{\tilde{L}} z_l z_{l-1} k_l^2\right). \quad (44)$$

which unveils the quadratic order of several system parameters and the neural network.

Remark 2: In this paper, we have designed a UWA-OFDM transceiver using fundamental modules such as the CNN-based channel estimator, the LDPC coding/decoding, and the interpolation-based channel reconstruction to design a transceiver for data transmission. The system design is validated using real channel measurements, including various losses and distortions.

IV. NUMERICAL RESULTS

The measurement data were collected from [44] and utilized to compute the channel features by the ℓ_p-norm optimization as in (15). The distance between two transducers is 100 [m], and the depth of the water is 10 [m]. In Fig. 5, the channel properties are visualized in both the time and frequency domains with the Doppler frequency $f_{\mathrm{D}} = 2$ [Hz] and $f_{\mathrm{D}} = 8$ [Hz]. We observe that all the channels are time-varying. However, Fig. 5(*a*) and Fig. 5(*b*) show the slow time-varying channels in the time and frequency domain, respectively. Meanwhile, Fig. 5(*c*) and Fig. 5(*d*) indicate the fast time-varying channels whose amplitudes are attenuated rapidly after a few paths. Moreover, the random fluctuations of fast time-varying channels are much more than those of slow time-varying channels as shown in Fig. 5(*b*) and Fig. 5(*d*).

For the evaluations of the system performance, we consider an UWA-OFDM system with the operation bandwidth 8 [kHz]. The number of subcarriers is 256 and the guard interval includes 60 samples. Both the Doppler frequency and the power delay profile are based on the measurement data. The CNN architecture is given in Table. 2. In the traing stage, the Adam method is exploited as the optimizer with the learning rate 0.0001. The number of epochs is 20 and the mini-batch size is 32. The validation patience is 10. In order to train and test the considered CNN model, a dataset comprising the 12000 realizations of the instantaneous channels was gathered. Specifically, the 8400 realizations utilized for the training stage, the 1800 realizations for the validation stage, and the 1800 realizations for the testing stage.

TABLE 2. CNN Architecture model for channel estimation.

Layer	Size	Activation function
InputLayer	30×377	–
Conv1Layer	$3 \times 3 \times 64$	ReLU
Conv2Layer	$3 \times 3 \times 64$	ReLU
Conv3Layer	$3 \times 3 \times 64$	ReLU
Conv4Layer	$3 \times 3 \times 64$	ReLU
LinearLayer	30×377	–

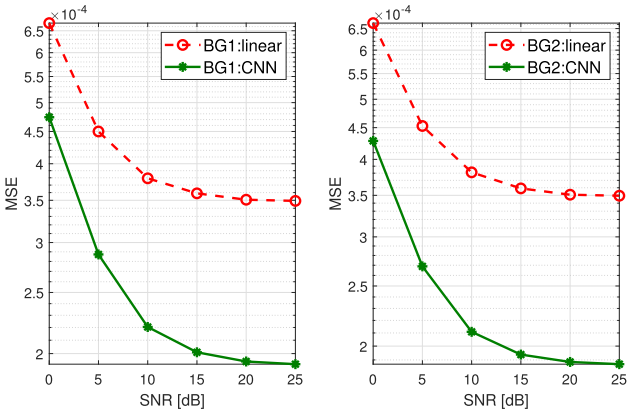

FIGURE 6. MSE of the channel estimation versus the SNR with the maximum Doppler frequency $f_{\mathrm{D,max}} = 8$ [Hz] and and QPSK.

We plot the mean square error (MSE) of the channel estimation with the Doppler frequency and different modulation schemes as in Figs. 6–8. The results demonstrate the effectiveness of the LPDC channel coding in providing high channel estimation quality. For all the parameter settings, the MSE is quite low, even with the high noise power. Moreover, the MSE drastically increases with the modulation index. For example, the MSE gets worse about one fold at the SNR 0 [dB] as the modulation index increases from 4 to 16. Furthermore, our proposed deep learning estimator yields better MSE performance than the conventional method exploiting linear interpolation. Superior improvements are observed, especially when the SNR grows up. The benefits of deep learning come from the effective exploitation of channel state information in the dataset.

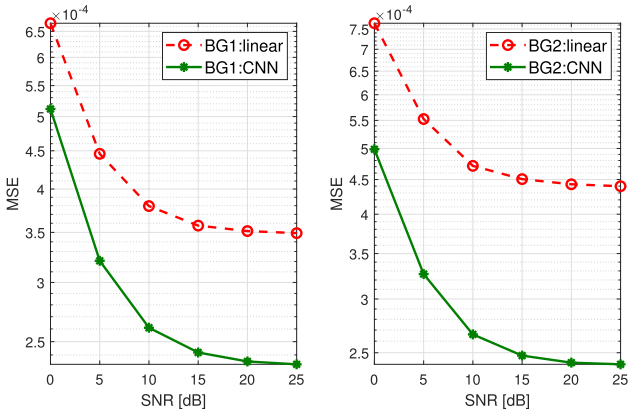

FIGURE 7. MSE of the channel estimation versus the SNR with the maximum Doppler frequency $f_{D,max} = 8$ [Hz] and 16 QAM.

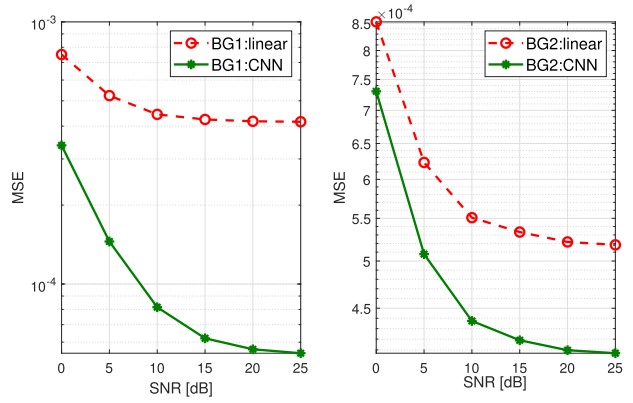

FIGURE 8. MSE of the channel estimation versus the SNR with the maximum Doppler frequency $f_{D,max} = 8$ [Hz] and 64 QAM.

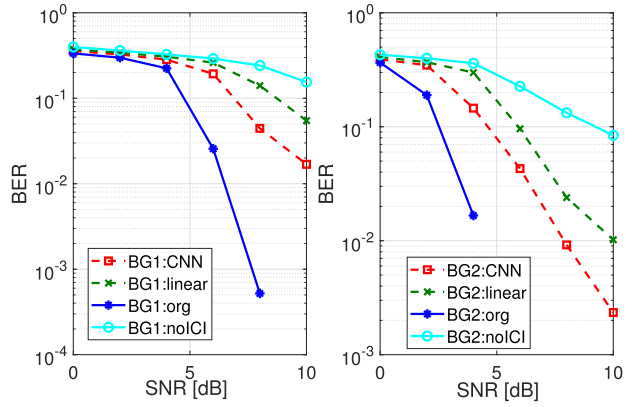

FIGURE 9. BER versus the SNR with the maximum Doppler frequency $f_{D,max} = 8$ [Hz] and QPSK.

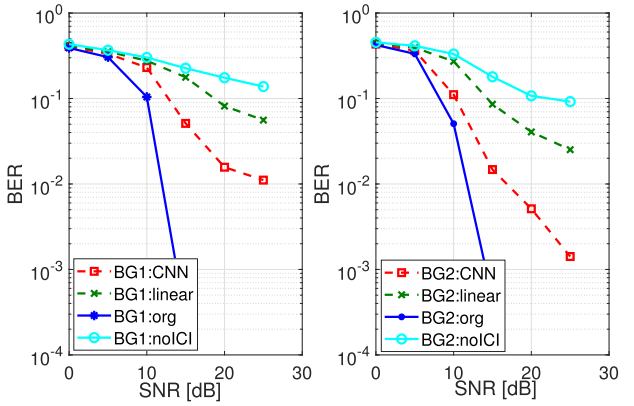

FIGURE 10. BER versus the SNR with the maximum Doppler frequency of $f_{D,max} = 8$ [Hz] and 16-QAM.

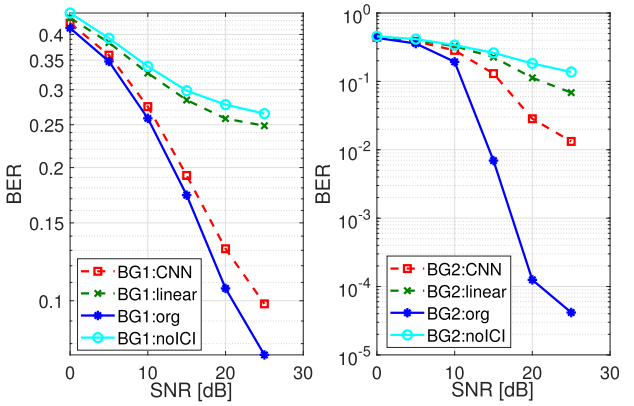

FIGURE 11. BER versus the SNR with the maximum Doppler frequency of $f_{D,max} = 8$ [Hz] and 64-QAM.

In Figs. 9-11, we show the BER performance of different modulations with two kinds of LDPC encoded schemes. Although the MSE of the two systems with different LPDC parameter settings is in small ranges, i.e., in the order of 10^{-4}, the BER of these systems is significant. The improvement of the BER performance by increasing the signal strength is aligned with that of the MSE performance. It means that the BER decreases gradually when the SNR increases, as displayed in Figs. 9-11. If the modulation level gets higher, the BER will decrease because it is more difficult for the receiver to separate the signal from the noise. With both the modulation indices, the BER values of the system using the BG2 matrix for encoding shows better performance than what the BG1 matrix has done. This can be explained by the code rate defined in two encoding schemes. Specifically, the BG1 is targeted for high data rates and small code lengths. In contrast, the BG2 matrix is targeted for low data rates and large code lengths. The more parity bits produce, the higher accuracy due to the LDPC decoder module. We also observe that the effects of inter-carrier interference are very significant in the UWA environment. Consequently, if the system does not utilize the channel equalizer, the BER is higher than the other benchmarks. For the three benchmarks exploiting the inter-carrier interference cancellation matrix, the BER of the considered system is better than the conventional least squares.

Next, we plot the BER performance as a function of the SNR with a lower Doppler frequency, say $f_{D,max} = 2$ [Hz], which is illustrated in Fig. 12. The BER is much better than the scenarios $f_{D,max} = 8$ [Hz]. However, there are some significant differences: There is no difference between the benchmarks using the inter-carrier interference cancellation matrix. The small Doppler frequency in this

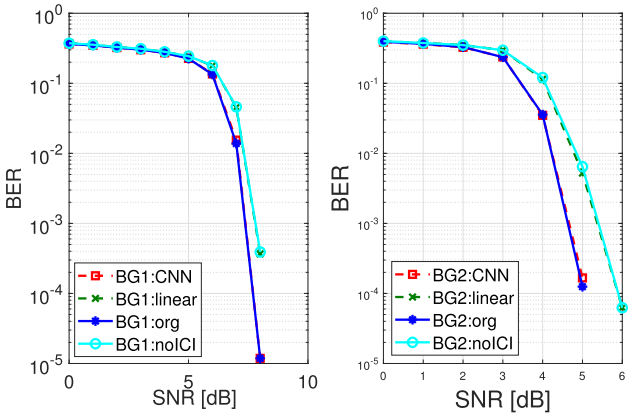

FIGURE 12. BER versus the SNR with the maximum Doppler frequency of $f_{D,max} = 2$ [Hz] and 16-QAM.

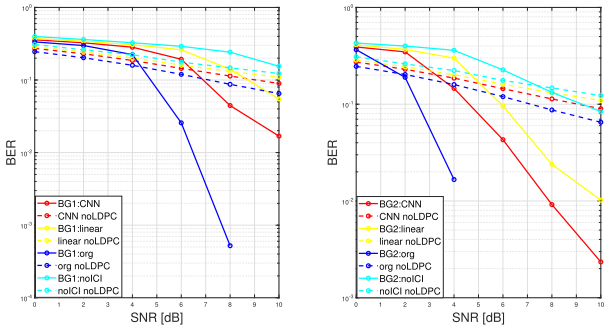

FIGURE 13. BER versus the SNR of the scenarios with and without the LDPC for a system having the maximum Doppler frequency $f_{D,max} = 8$ [Hz] and QPSK.

scenario makes the effects of inter-carrier interference effect not significant. Another critical point is that the CNN model works productively and fits the data well. Hence, the quality of the channel estimates is very accurate and close to the true channels. It leads to the BER of these benchmarks are almost overlapped with each other.

In Fig. 13, we show the BER performance using the QPSK modulations with the two considered LDPC encoded/decoded schemes. The system exploiting the LDPC schemes and CNN-based channel estimator performs better than the remaining benchmarks. As the channel estimation errors are reduced thanks to the CNN-based channel estimator, the LDPC decoder will detect data symbols more precisely. The system gains much better BER than the system exploits only CNN-based channel estimator without the support of the LPDC.

V. CONCLUSION

This paper has manifested the effectiveness of the data-driven method in channel estimation for UWA communications. Motivated by the recent report of 3GPP, the LDPC code has been exploited to boost communication reliability. The least squares estimation initially obtains the channel estimates in the time domain. After that, the supervised learning and the ℓ_p-norm optimization cooperated in training a CNN from real channel measurements. We have demonstrated the superior improvements of the proposed system model by extensive numerical results under different system parameter settings. Extensions of our framework to multiple-input multiple-output (MIMO) UWA systems with different neural network architectures are potential extensions of interest in this work.

REFERENCES

[1] J. Zhang, G. Han, J. Sha, Y. Qian, and J. Liu, "AUV-assisted subsea exploration method in 6G enabled deep ocean based on a cooperative pac-men mechanism," *IEEE Trans. Intell. Transp. Syst.*, vol. 23, no. 2, pp. 1649–1660, Feb. 2022.

[2] A. Higuchi, E. Takeshita, D. Hisano, Y. Inoue, K. Maruta, T. Nishio, Y. Hara-Azumi, and Y. Nakayama, "Aquatic fronthaul for underwater-ground communication in 6G mobile communications," in *Proc. IEEE 95th Veh. Technol. Conf. (VTC-Spring)*, Jun. 2022, pp. 1–6.

[3] P. Singh, V. A. Bohara, and A. Srivastava, "On the optimization of integrated terrestrial-air-underwater architecture using optical wireless communication for future 6G network," *IEEE Photon. J.*, vol. 14, no. 6, pp. 1–12, Dec. 2022.

[4] D. C. Nguyen, M. Ding, P. N. Pathirana, A. Seneviratne, J. Li, D. Niyato, O. Dobre, and H. V. Poor, "6G Internet of Things: A comprehensive survey," *IEEE Internet Things J.*, vol. 9, no. 1, pp. 359–383, Jan. 2022.

[5] P. A. van Walree, "Propagation and scattering effects in underwater acoustic communication channels," *IEEE J. Ocean. Eng.*, vol. 38, no. 4, pp. 614–631, Oct. 2013.

[6] P. Qarabaqi and M. Stojanovic, "Statistical characterization and computationally efficient modeling of a class of underwater acoustic communication channels," *IEEE J. Ocean. Eng.*, vol. 38, no. 4, pp. 701–717, Oct. 2013.

[7] D. V. Ha, N. T. H. Linh, N. T. Nga, and N. Van Duc, "On optimizing guard interval lengths for UWA-OFDM communication systems using geometry-based channel modelling," in *Proc. IEEE 8th Int. Conf. Commun. Electron. (ICCE)*, Jan. 2021, pp. 18–23.

[8] J. Ahn, H. Lee, Y. Kim, and J. Chung, "Snapping shrimp noise detection and mitigation for underwater acoustic orthogonal frequency division multiple communication using multilayer frequency," *Int. J. Nav. Archit. Ocean Eng.*, vol. 12, pp. 258–269, Jan. 2020.

[9] P. Kotipalli, M. A. S. M. Mohanraju, and P. Vardhanapu, "Frame boundary detection and deep learning-based Doppler shift estimation for FBMC/OQAM communication system in underwater acoustic channels," *IEEE Access*, vol. 10, pp. 17590–17608, 2022.

[10] D. Tollefsen, W. S. Hodgkiss, S. E. Dosso, J. Bonnel, and D. P. Knobles, "Probabilistic estimation of merchant ship source levels in an uncertain shallow-water environment," *IEEE J. Ocean. Eng.*, vol. 47, no. 3, pp. 647–656, Jul. 2022.

[11] G. Yang, Q. Guo, H. Ding, Q. Yan, and D. D. Huang, "Joint message-passing-based bidirectional channel estimation and equalization with superimposed training for underwater acoustic communications," *IEEE J. Ocean. Eng.*, vol. 46, no. 4, pp. 1463–1476, Oct. 2021.

[12] M. Murad, I. A. Tasadduq, and P. Otero, "Pilots based LSE channel estimation for underwater acoustic OFDM communication," in *Proc. Global Conf. Wireless Opt. Technol. (GCWOT)*, Oct. 2020, pp. 1–6.

[13] B. Wang and X. Guan, "Channel estimation for underwater acoustic communications based on orthogonal chirp division multiplexing," *IEEE Signal Process. Lett.*, vol. 28, pp. 1883–1887, 2021.

[14] X. Feng, J. Wang, X. Kuai, M. Zhou, H. Sun, and J. Li, "Message passing-based impulsive noise mitigation and channel estimation for underwater acoustic OFDM communications," *IEEE Trans. Veh. Technol.*, vol. 71, no. 1, pp. 611–625, Jan. 2022.

[15] A. L. Ha, T. Van Chien, T. H. Nguyen, W. Choi, and V. D. Nguyen, "Deep learning-aided 5G channel estimation," in *Proc. 15th Int. Conf. Ubiquitous Inf. Manage. Commun. (IMCOM)*, Jan. 2021, pp. 1–7.

[16] X. Cai, W. Xu, L. Wang, and G. Kaddoum, "Joint energy and correlation detection assisted non-coherent OFDM-DCSK system for underwater acoustic communications," *IEEE Trans. Commun.*, vol. 70, no. 6, pp. 3742–3759, Jun. 2022.

[17] Y. Zhang, R. Venkatesan, O. A. Dobre, and C. Li, "Efficient estimation and prediction for sparse time-varying underwater acoustic channels," *IEEE J. Ocean. Eng.*, vol. 45, no. 3, pp. 1112–1125, Jul. 2020.

[18] E. Panayirci, M. T. Altabbaa, and H. V. Poor, "Channel estimation and equalization for Alamouti SF-coded OFDM-UWA communications," *IEEE Trans. Veh. Technol.*, vol. 70, no. 2, pp. 1709–1723, Feb. 2021.
[19] M. Rawat, B. Lall, and S. Srirangarajan, "Angle of arrival distribution in an underwater acoustic communication channel with incoherent scattering," *IEEE Access*, vol. 8, pp. 133204–133211, 2020.
[20] S. Zhao, S. Yan, and J. Xi, "Adaptive turbo equalization for differential OFDM systems in underwater acoustic communications," *IEEE Trans. Veh. Technol.*, vol. 69, no. 11, pp. 13937–13941, Nov. 2020.
[21] A. Goalic, J. Trubuil, and N. Beuzelin, "Channel coding for underwater acoustic communication system," in *Proc. OCEANS*, Sep. 2006, pp. 1–4.
[22] I. Karasalo, T. Öberg, B. Nilsson, and S. Ivansson, "A single-carrier turbo-coded system for underwater communications," *IEEE J. Ocean. Eng.*, vol. 38, no. 4, pp. 666–677, Oct. 2013.
[23] B. Tahir, S. Schwarz, and M. Rupp, "BER comparison between convolutional, turbo, LDPC, and polar codes," in *Proc. 24th Int. Conf. Telecommun. (ICT)*, May 2017, pp. 1–7.
[24] X.-K. Qi, Y. Li, and H.-N. Huang, "Construction of reversible QC-LDPC codes and its performance in underwater acoustic communication system," *J. Electron. Inf. Technol.*, vol. 34, no. 8, pp. 1986–1992, Jul. 2013.
[25] H. Li, B. Bai, X. Mu, J. Zhang, and H. Xu, "Algebra-assisted construction of quasi-cyclic LDPC codes for 5G new radio," *IEEE Access*, vol. 6, pp. 50229–50244, 2018.
[26] T. Van Chien, E. Björnson, and E. G. Larsson, "Joint power allocation and load balancing optimization for energy-efficient cell-free massive MIMO networks," *IEEE Trans. Wireless Commun.*, vol. 19, no. 10, pp. 6798–6812, Oct. 2020.
[27] M. K. Shehzad, L. Rose, M. M. Butt, I. Z. Kovács, M. Assaad, and M. Guizani, "Artificial intelligence for 6G networks: Technology advancement and standardization," *IEEE Veh. Technol. Mag.*, vol. 17, no. 3, pp. 16–25, Sep. 2022.
[28] A. Ghazanfari, T. Van Chien, E. Björnson, and E. G. Larsson, "Model-based and data-driven approaches for downlink massive MIMO channel estimation," *IEEE Trans. Commun.*, vol. 70, no. 3, pp. 2085–2101, Mar. 2022.
[29] T.-Y. Tung and D. Gündüz, "DeepWiVe: Deep-learning-aided wireless video transmission," *IEEE J. Sel. Areas Commun.*, vol. 40, no. 9, pp. 2570–2583, Sep. 2022.
[30] T. T. Vu, T. Van Chien, C. T. Dinh, H. Q. Ngo, and M. Matthaiou, "Channel estimation in RIS-assisted downlink massive MIMO: A learning-based approach," in *Proc. IEEE 23rd Int. Workshop Signal Process. Adv. Wireless Commun. (SPAWC)*, Jul. 2022, pp. 1–5.
[31] J. Gao, C. Zhong, G. Y. Li, and Z. Zhang, "Deep learning-based channel estimation for massive MIMO with hybrid transceivers," *IEEE Trans. Wireless Commun.*, vol. 21, no. 7, pp. 5162–5174, Jul. 2022.
[32] T. Van Chien, T. N. Canh, E. Björnson, and E. G. Larsson, "Power control in cellular massive MIMO with varying user activity: A deep learning solution," *IEEE Trans. Wireless Commun.*, vol. 19, no. 9, pp. 5732–5748, Sep. 2020.
[33] J. Liu, F. Ji, H. Zhao, J. Li, and M. Wen, "CNN-based underwater acoustic OFDM communications over doubly-selective channels," in *Proc. IEEE 94th Veh. Technol. Conf. (VTC-Fall)*, Sep. 2021, pp. 1–6.
[34] Y. Zhang, C. Li, H. Wang, J. Wang, F. Yang, and F. Meriaudeau, "Deep learning aided OFDM receiver for underwater acoustic communications," *Appl. Acoust.*, vol. 187, Feb. 2022, Art. no. 108515.
[35] A. Lykartsis, M. Hädrich, and S. Weinzierl, "A prototype deep learning system for the acoustic monitoring of intensive care patients," in *Proc. 29th Eur. Signal Process. Conf. (EUSIPCO)*, Aug. 2021, pp. 980–984.
[36] A. Testolin, D. Kipnis, and R. Diamant, "Detecting submerged objects using active acoustics and deep neural networks: A test case for pelagic fish," *IEEE Trans. Mobile Comput.*, vol. 21, no. 8, pp. 2776–2788, Aug. 2022.
[37] D. V. Ha, H. Trung, and N. Van Duct, "Symbol duration and adaptive guard length for underwater acoustic OFDM systems," in *Proc. Int. Conf. Adv. Technol. Commun. (ATC)*, Oct. 2019, pp. 169–173.
[38] *Multiplexing and Channel Coding*, document 138 212, 3rd Generation Partnership Project (3GPP), 2018.
[39] M. Pätzold, *Mobile Radio Channels*. Hoboken, NJ, USA: Wiley, 2011.
[40] R.-S. Ran and T.-Z. Huang, "An inversion algorithm for a banded matrix," *Comput. Math. Appl.*, vol. 58, no. 9, pp. 1699–1710, Nov. 2009.
[41] X. Wu, M. Jiang, and C. Zhao, "Decoding optimization for 5G LDPC codes by machine learning," *IEEE Access*, vol. 6, pp. 50179–50186, 2018.
[42] W. G. Jeon, K. H. Chang, and Y. S. Cho, "An equalization technique for orthogonal frequency-division multiplexing systems in time-variant multipath channels," *IEEE Trans. Commun.*, vol. 47, no. 1, pp. 27–32, Jan. 1999.
[43] K. He and J. Sun, "Convolutional neural networks at constrained time cost," in *Proc. IEEE Conf. Comput. Vis. Pattern Recognit. (CVPR)*, Jun. 2015, pp. 5353–5360.
[44] D. V. Ha and N. V. Duc, "Analytical method of parameter determination for OFDM system over measurement-based underwater acoustic channel modeling," *Phys. Commun.*, vol. 40, Jun. 2020, Art. no. 101045.

VAN DUC NGUYEN was born in Thanh Hóa, Vietnam, in 1973. He received the bachelor's and master's degrees in electronics and communications from the Hanoi University of Technology, Vietnam, in 1995 and 1997, respectively, and the Dr.Eng. degree in communications engineering from the University of Hannover, Germany, in 2003. From 1995 to 1998, he was an Assistant Researcher with the Technical University of Hanoi. In 1996, he participated in the Student Exchange Program between the Technical University of Hanoi and the Munich University of Applied Sciences for one term. From 1998 to 2003, he was with the Institute of Communications Engineering, University of Hannover, first as a DAAD Scholarship Holder and then as a member of the Scientific Staff. From 2003 to 2004, he was a Postdoctoral Researcher with the Agder University College, Grimstad, Norway. He was also a Postdoctoral Fellow with the International University of Bremen. In 2007, he spent two months with Sungkyungkwan University, South Korea, as a Research Professor. In 2008, he was a Visiting Researcher with Klagenfurt University, Austria. In 2009, he was a Visiting Researcher with Agder University, Norway. His current research interests include mobile radio communications, especially MIMO-OFDM systems, and radio resource management, channel coding for cellular, and ad-hoc networks.

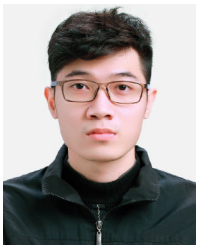

DINH KHOA PHAN received the B.S. degree in electronic and telecommunications engineering from the Hanoi University of Science and Technology (HUST), Hanoi, Vietnam, in 2022, where he is currently pursuing the master's degree in telecommunication engineering. His current research interest includes machine learning for wireless communication systems.

TRINH VAN CHIEN (Member, IEEE) received the B.S. degree in electronics and telecommunications from the Hanoi University of Science and Technology (HUST), Vietnam, in 2012, and the M.S. degree in electrical and computer engineering from Sungkyunkwan University (SKKU), South Korea, in 2014, and the Ph.D. degree in communication systems from Linköping University (LiU), Sweden, in 2020. He was a Research Associate with the University of Luxembourg. He is currently with the School of Information and Communication Technology (SoICT), HUST. His research interests include convex optimization problems and machine learning applications for wireless communications and image and video processing. He was a recipient of the Award of Scientific Excellence in the first year of the 5G Wireless Project funded by the European Union Horizon's 2020. He was an exemplary Reviewer of IEEE Wireless Communications Letters, in 2016, 2017, and 2021.